Progress In Electromagnetics Research, PIER 96, 251–266, 2009

FAST CAPACITANCE EXTRACTION FOR FINITE PLANAR PERIODIC STRUCTURES USING THE GENERALIZED FORWARD-BACKWARD AND NOVEL SPECTRAL ACCELERATION METHOD

C. Lertsirimit and D. Torrungrueng

Department of Electrical and Electronic Engineering
Faculty of Engineering and Technology
Asian University
Chon Buri 20150, Thailand

Abstract—The generalized forward-backward and novel spectral acceleration (GFB/NSA) method is applied to capacitance extraction problems of finite planar periodic structures. In the GFB method, the interaction within a unit cell can be calculated and stored beforehand. The interactions between relatively far-separated unit cells are however calculated by the GFB/NSA method to further accelerate the calculation speed. The contributions to a receiving element on finite planar periodic structures are separated into weak and strong source contributions by an appropriate separation index, which is conveniently specified by an amount of unit cells rather than a distance. The strong source contribution is performed by the standard matrix-vector multiplication in the GFB method, while the weak source contribution is computed using the NSA algorithm. Numerical examples show comparisons of the GFB/NSA method with a commercial software, including the efficiency of the method. With the array increment in one direction, the GFB/NSA method shows $\mathcal{O}(N)$ in the calculation time per iteration, while its memory requirement for a very large problem also tends to be $\mathcal{O}(N)$, where N is the number of unknowns.

1. INTRODUCTION

Capacitance extraction problems in three-dimensional structures have been studied extensively [1–14]. There are several methods to accelerate the calculation of these problems [3–14]. One of them is

Corresponding author: C. Lertsirimit (chatrpol@gmail.com).

the forward-backward (FB) method [12] illustrating an $\mathcal{O}(N^2)$ matrix-vector multiplication calculation time per iteration, where N is the number of unknowns. The method combined with the novel spectral acceleration (NSA) algorithm can further speed up the calculation time to $\mathcal{O}(N)$ [13–17]. However, the FB and FB/NSA methods generally converge rapidly only for smoothly varying surfaces or the surfaces without vertically-overlapping regions. Without smoothly varying surfaces, the FB and FB/NSA methods are expected to have slow convergent behavior or no convergence at all. The generalized forward-backward (GFB) method is then used to overcome this convergent problem [18–20]. The GFB method has been used successfully in rough surfaces scattering problems incorporating ships or breaking waves in the structures [18, 19], while the method used in capacitance extraction problems [20] exhibits faster convergent rates than that of the FB method. In contrast to the FB method, the GFB method solves the system matrix by using subblocks for the associated unknown quantities in the overlapping regions. This construction of the submatrix is also suitable for array problems since each subblock can represent interactions within a unit cell. Thus, some repetitive calculations can be performed and stored beforehand. The interactions between relatively far-separated unit cells are however calculated by the GFB/NSA method to significantly accelerate the calculation speed.

In this paper, we apply the GFB/NSA method to capacitance extraction of planar periodic structures. Numerical experiments demonstrate that the memory requirement and computational complexity of the present method can be reduced to approximately $\mathcal{O}(N)$ for the array increment in one direction.

2. THE METHOD OF MOMENTS AND THE GFB METHOD

For illustration, consider N_u conducting patches arranged in planar periodic structures in free space as shown in Fig. 1. There are N_x and N_y conducting patches in the x- and y-directions, respectively. The finite periodic array having a cell size of $w_c \times l_c\,\mathrm{m}^2$ is located at $z = 0\,\mathrm{m}$. For convenience in illustration, a conducting patch having a size of $w \times l\,\mathrm{m}^2$ is located at the center of the unit cell and separated at a distance $d/2$ from each edge of the unit cell. The maximum distance from the leftmost to the rightmost patches is defined as D_x while that from the bottom to the top patches is D_y, as shown in Fig. 1. A potential, V, applied to the conducting patches is related to

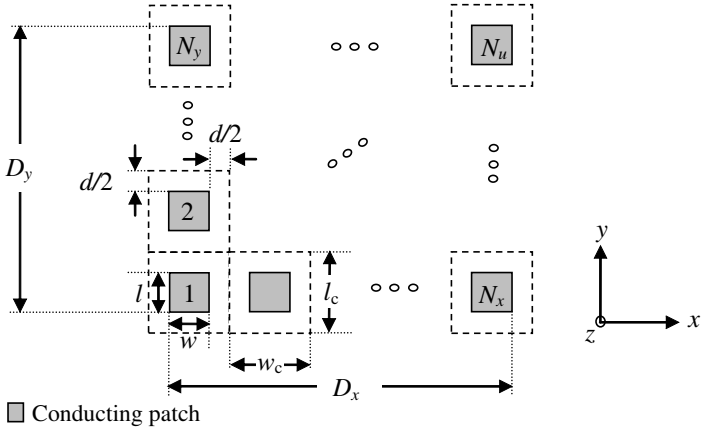

Figure 1. A planar structure consists of a finite periodic array of conducting patches in free space.

the unknown surface charge density, ρ_s, as [21]

$$V(\bar{r}) = \int_S \left(\frac{\rho_s(\bar{r}')}{4\pi\varepsilon_0 |\bar{r} - \bar{r}'|} \right) ds', \tag{1}$$

where S are the surfaces of all the conducting patches, $\bar{r} = x\hat{x} + y\hat{y} + z\hat{z}$ is the position vector of a receiving point, and $\bar{r}' = x'\hat{x} + y'\hat{y} + z'\hat{z}$ is that of a source point. To find the unknown surface charge densities in the method of moments, each patch in a unit cell is discretized into smaller areas with the total of N_p elements per unit cell. Therefore, the total number of elements used in the method of moments is equal to $N = N_p \times N_u$, where $N_u = N_x \times N_y$. Using the pulse basis and point matching results in the following equation [21]:

$$\overline{\overline{Z}}\,\overline{I} = \overline{V}, \tag{2}$$

where $\overline{\overline{Z}}$ denotes the method of moments matrix, $\overline{V}$ is the vector containing applied potentials, $\overline{I}$ is the vector containing unknown surface charge densities. The unknown surface charge densities are then solved by the iterative GFB method.

To start the GFB algorithm, the unknown surface charge density vector, $\bar{I}$, is expressed as the sum of two contributions

$$\overline{I} = \overline{I}^f + \overline{I}^b, \tag{3}$$

where $\overline{I}^f$ and $\overline{I}^b$ are the unknown surface charge density vectors of the forward and backward iterations, respectively. In addition, the matrix

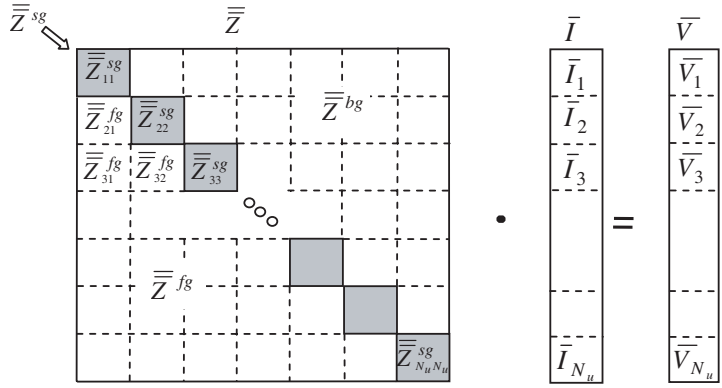

Figure 2. An example of the matrix decomposition for the GFB method.

$\bar{\bar{Z}}$ is split as

$$\bar{\bar{Z}} = \bar{\bar{Z}}^{fg} + \bar{\bar{Z}}^{sg} + \bar{\bar{Z}}^{bg}, \tag{4}$$

where $\bar{\bar{Z}}^{sg}$ matrix is the diagonal part of $\bar{\bar{Z}}$ with additional blocks including the impedance submatrices corresponding to the interactions within unit cells. The matrices $\bar{\bar{Z}}^{fg}$ and $\bar{\bar{Z}}^{bg}$ are the lower and upper triangular parts of $\bar{\bar{Z}}$ but excluding the matrix $\bar{\bar{Z}}^{sg}$, respectively. Fig. 2 illustrates an example of the matrix decomposition for the GFB method.

The matrix $\bar{\bar{Z}}^{sg}$ has been subdivided into smaller square matrices, $\bar{\bar{Z}}^{sg}_{ii}$ $(i = 1, 2, \ldots, N_u)$ corresponding to the interaction within the ith unit cell. The matrix $\bar{\bar{Z}}^{fg}$ (or $\bar{\bar{Z}}^{bg}$) is also subdivided into smaller square matrices, where $\bar{\bar{Z}}^{fg}_{ij}$ (or $\bar{\bar{Z}}^{bg}_{ij}$) corresponds to the interaction from the jth unit cell to the ith unit cell. The surface charge density vector and the potential vector are subdivided into smaller vectors, $\bar{I}_i$ and $\bar{V}_i$ corresponding to unknown surface charge densities and given potentials of the ith unit cell, respectively. In the GFB algorithm, the unknown surface charge density vectors for the kth iteration are calculated as

$$\bar{I}_i^{f,(k)} = \bar{\bar{Z}}_{ii}^{sg^{-1}} \left[\bar{V}_i - \sum_{j=1}^{i-1} \bar{\bar{Z}}_{ij}^{fg} \left(\bar{I}_j^{f,(k)} + \bar{I}_j^{b,(k-1)} \right) \right], \tag{5}$$

$$\bar{I}_i^{b,(k)} = -\bar{\bar{Z}}_{ii}^{sg^{-1}} \left[\sum_{j=i+1}^{N_u} \bar{\bar{Z}}_{ij}^{bg} \left(\bar{I}_j^{f,(k)} + \bar{I}_j^{b,(k)} \right) \right], \tag{6}$$

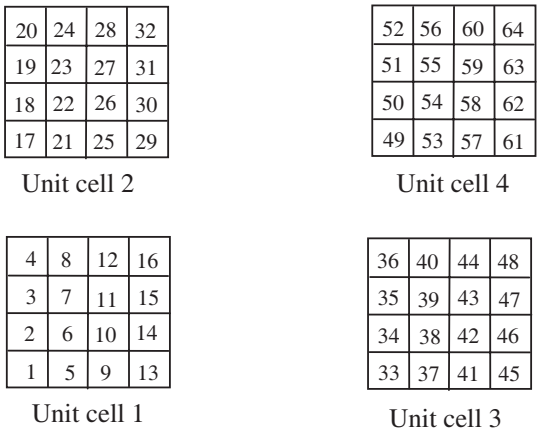

Figure 3. An illustration of the proposed numbering scheme for four unit cells of conducting patches.

where $i = 2, 3, \ldots, N_u$ in (5) and $i = (N_u - 1), (N_u - 2), \ldots, 1$ in (6). Both (5) and (6) are systems of linear equations for computing the surface charge densities of the ith unit cell in the forward and backward iterations, respectively. Thus, there are $(N_u - 1)$ systems of equations to be solved in both forward and backward iterations. The inverse matrix $\bar{\bar{Z}}^{sg^{-1}}$ can be computed and stored beforehand, thus reducing the computational time in subsequent iterations and for other excitations. Note that $\bar{I}_1^{f,(1)}$ can be computed and stored to use at other iterations ($\bar{I}_1^{f,(k)} = \bar{I}_1^{f,(1)}$) while $\bar{I}_{N_u}^{b,(k)}$ are set to zero for all iterations.

Due to the three-dimensional nature of the problem, care must be taken in forming the matrix $\bar{\bar{Z}}$ and the submatrices [20]. In this paper, the numbering scheme is finished within the unit cell before moving to the next unit cell from bottom to top and from left to right. Within the unit cell, the numbering scheme also runs from bottom to top and then from left to right. Fig. 3 illustrates an example of the above numbering scheme for four unit cells. Each unit cell has one conducting patch subdivided into 16 subsections.

3. THE NOVEL SPECTRAL ACCELERATION METHOD

The novel spectral acceleration method for fast capacitance extraction has been successfully applied in [13, 14]. In this paper, we apply the NSA method to finite planar periodic structure problems. For

convenience in discussion, we refer to the ith unit cell as a receiving cell and the jth unit cell as a source cell. In addition, source cells are categorized as strong sources, for those in a close vicinity of the receiving cell, and weak sources for those separated from the receiving cell. Then, the potential at the ith unit cell in (1) can be decomposed as

$$\overline{V}_i(\bar{r}) = \bar{V}_i^s(\bar{r}) + \bar{V}_i^w(\bar{r}), \tag{7}$$

where $\bar{V}_i^s(\bar{r})$ and $\bar{V}_i^w(\bar{r})$ are the potentials at the receiving cell due to the strong and weak sources, respectively. This separation leads to the decomposition of the source cells in (5); $j = 1, 2, \ldots, N_w$ for the weak sources and $j = (N_w + 1), (N_w + 2), \ldots, (i - 1)$ for the strong sources. A cell separation index in the x-direction, L_x, between the strong and the weak sources is defined as

$$L_x = floor\left|\frac{i - 1 - N_w}{N_y}\right|, \tag{8}$$

for the generalized forward iteration. The cell separation index is specified by users to indicate the size of the strong sources. The potential due to the strong sources is calculated by the standard matrix-vector multiplication in the GFB method described in the previous section while the potential due to the weak sources is calculated by the NSA algorithm. Fig. 4 shows an example of a 6×3 array with $L_x = 1$. The receiving element is the 11th element. The strong and weak sources in the generalized forward iteration are the 7th to 10th elements and the 1th to 6th elements, respectively.

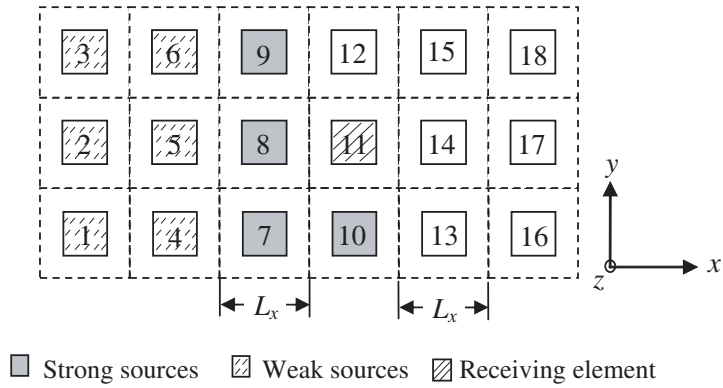

Figure 4. An illustration of the separation of the strong and weak sources in the generalized forward iteration.

To employ the NSA method, first consider (1) in the form of the free-space Green's function $G(\bar{r}, \bar{r}')$,

$$V(\bar{r}) = \int_S \rho_s(\bar{r}') G(\bar{r}, \bar{r}') ds', \tag{9}$$

where

$$G(\bar{r}, \bar{r}') = \frac{1}{4\pi\varepsilon_0 |\bar{r} - \bar{r}'|}. \tag{10}$$

The weak source contribution can be efficiently computed by employing the spectral representation of the free-space Green's function in (10) in polar form as [13]

$$G(\bar{r}, \bar{r}') = \frac{1}{8\pi^2\varepsilon_0} \int_0^{2\pi} \int_0^{\infty} \left[e^{-k_\rho |x-x'|} e^{jk_\rho (y-y')\cos\alpha} e^{jk_\rho (z-z')\sin\alpha} \right] dk_\rho d\alpha. \tag{11}$$

Note that the integrand in (11) possesses an exponential decay factor in the integrand as a function of the separation of the weak source point and the receiving point in the x-direction. On the iterative scheme, the potential at the mth subelement in the ith unit cell, $V_{i,m}^{w,(k)}(\bar{r})$, due to all weak sources in the jth unit cell on the kth iteration can be expressed compactly as

$$V_{i,m}^{w,(k)}(\bar{r}) = \frac{1}{8\pi^2\varepsilon_0} \int_0^{\infty} dk_\rho \int_0^{2\pi} d\alpha \cdot F^{(k)}(\bar{r}, \bar{r}', k_\rho, \alpha), \tag{12}$$

where $F^{(k)}(\bar{r}, \bar{r}', k_\rho, \alpha)$ is called the complex scalar spectral function on the kth iteration defined as

$$F^{(k)}(\bar{r}, \bar{r}', k_\rho, \alpha) = \int_{S_j} ds' \rho_s^{(k)}(\bar{r}') e^{-k_\rho (x-x')} e^{jk_\rho [(y-y')\cos\alpha + (z-z')\sin\alpha]}, \tag{13}$$

for the forward iteration. Note that S_j in (13) is the surface of all weak sources in the jth unit cell. It should be pointed out that the complex scalar spectral function has a recursive property, and its computation can be performed through a "phase shifting" process [16].

Figure 5 illustrates the matrix $\bar{\bar{Z}}^{fg}$ for the generalized forward iteration for the example in Fig. 4. Note that the forming of $\bar{\bar{Z}}^{fg}$ starts with the receiving element moving from bottom to top and left to right. The NSA method in this example starts when the receiving element is at the 7th unit cell. Then, the number of the weak sources increases to the maximum number of twelve unit cells as the receiving

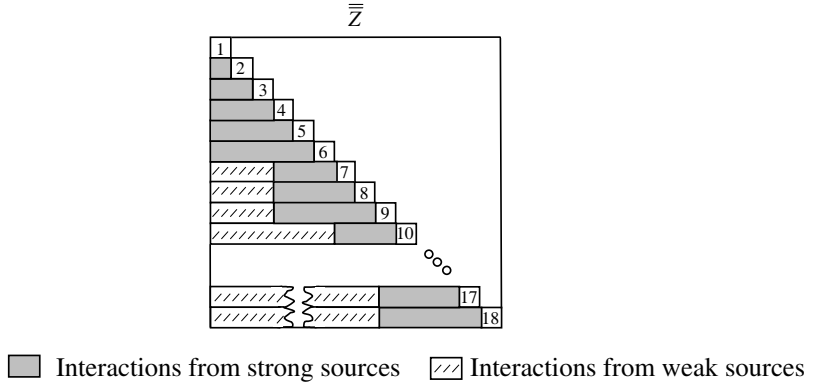

Figure 5. An impedance matrix for the generalized forward iteration of the example in Fig. 4.

element moves in the forward fashion. A number of the strong sources, however, vary from one to five unit cells. The decomposition of the source cells in (6) for the backward iteration and the matrix $\bar{\bar{Z}}^{bg}$ can be performed similarly.

Any numerical integration scheme can be employed in (12). The complex scalar spectral function is required to be stored and updated. Therefore, the total number of integration points associated with the spectral function affects the speed and storage of the NSA algorithm, and care must be taken for the integrals in k_ρ and α in (12). Firstly, the integrations must cover sufficient range so that their integrands converge. Secondly, to use a numerical integration scheme, the integrals must be divided into a sufficiently small interval for acceptable accuracy. Note that increasing the total number of integration points results in slower computational time and larger required storage. Thus, a careful study is required to obtain the optimum integration points with acceptable accuracy.

4. COMPUTATIONAL COST AND MEMORY STORAGE REQUIREMENT OF THE GFB/NSA METHOD

The computational cost for the generalized forward-backward method is $\mathcal{O}(N^2)$ per iteration [18]. In the following analysis, we estimate the computational cost and memory storage requirement while assuming that the number of unit cell in the y-direction, N_y, is fixed. In the generalized forward-backward with the spectral acceleration method, the operational count to compute the strong region contribution for

total receiving points, N, is C_sN_sN, where N_s is approximately the number of sources in the strong region and C_s is a proportional constant. In addition, the operational count in computing the weak region contribution is $C_wQ_{TOT}(N - N_s)$, where Q_{TOT} is the total number of integration points in k_ρ and α planes in (12) and C_w is an additional proportional constant. Thus, the total operational count, $\mathcal{C}$, can be estimated as

$$\mathcal{C} \approx C_sN_sN + C_w\,Q_{TOT}(N - N_s). \tag{14}$$

Since L_x is fixed, N_s is not a function of N. In addition, Q_{TOT} is not a function of N either due to the fact that N_y and L_x are fixed. Thus, (14) implies that the total operational count is $\mathcal{O}(N)$ per iteration.

The total memory storage requirement, $\mathcal{M}$, of this method is estimated as

$$\mathcal{M} \approx C_NN + C_QQ_{TOT}, \tag{15}$$

where C_NN indicates the memory requirement of the generalized forward-backward method, C_QQ_{TOT} is the storage for all the integration points needed in evaluating (12), and C_N and C_Q are proportional constants. It is noted from (15) that there is no storage for matrix elements associated with the strong region since they are recalculated for each iteration to reduce the overall memory storage. If the total number of the receiving element, N, is much larger than the total integration points, Q_{TOT}, then $\mathcal{M}$ is dominated by the first term in (15). Therefore, for fixed N_y and L_x, it can be concluded from (15) that $\mathcal{M}$ is $\mathcal{O}(N)$.

5. NUMERICAL RESULTS

Consider a planar finite periodic array of $N_x \times N_y$ cells as shown in Fig. 1 with the following geometry: $w = 1\,\text{mm}$, $l = 1\,\text{mm}$, $d = 1\,\text{mm}$, $w_c = 2\,\text{mm}$ and $l_c = 2\,\text{mm}$. In each unit cell, the conducting patch is discretized uniformly into 20×20 subsections. These conducting patches are used in the following examples. Note that the calculation is performed by Pentium Celeron CPU 3.0 GHz with 512 MB RAM.

The first example calculates the electrostatic-induction coefficients to be compared with those calculated by the ES3D [22] to check the accuracy of the GFB/NSA method. There are 5×3 unit cells with the total unknowns of 6,000. The electrostatic-induction coefficient is defined as

$$b_{ij} = \left.\frac{Q_i}{V_j}\right|_{V_k=0,\,k=1,\ldots,N_u,\;k\neq j}, \tag{16}$$

Table 1. Comparisons of the accuracy and the computational time of each method.

Parameters \ Methods	ES3D [22]	GFB	GFB/NSA $L_x = 1$
Relative error ε_b (%)	—	1.27	1.27
Number of iterations	—	4	4
Total time (s)	355	2,490	10,482

where Q_i is the total charges on the ith patch and V_j is the potential applied at the jth patch while all other patches are set to zero (ground). The GFB/NSA method employs one unit cell $L_x = 1$ as the separation index of the strong and the weak regions. The relative electrostatic-induction error in percent, ε_b, is calculated in the root mean square sense,

$$\varepsilon_b(\%) = \frac{100}{N_u}\sqrt{\sum_{j=1}^{N_u}\sum_{i=1}^{N_u}\left(\frac{b_{ij}-\tilde{b}_{ij}}{b_{ij}}\right)^2}, \tag{17}$$

where b_{ij} is the electrostatic-induction coefficient calculated by the ES3D, $\tilde{b}_{ij}$ is the electrostatic-induction coefficient calculated by the GFB or GFB/NSA methods, and N_u is the total number of patches ($N_u = 15$).

Table 1 shows the comparisons of the ES3D, the GFB and GFB/NSA methods. Note that both GFB and GFB/NSA methods have the same relative error; i.e., the NSA algorithm still keeps the accuracy at the same level as the GFB method. In addition, both of them use the same number of iterations to converge. This is to be expected if the NSA calculation yields the same weak contributions as those from the GFB calculation. However, the computational time of the GFB/NSA method is much longer than that of the GFB method since the additional NSA computation is relatively large compared to the overall calculation for this relatively small problem.

The second example compares the accuracy and speed of the GFB and GFB/NSA methods. The same unit cell and discretization as in the first example are applied here. In this example, the number of unit cell in the y-direction, N_y, is fixed at five while the numbers of unit cell in the x-direction, N_x, are varied to 10, 50, 100 and the total numbers of unknowns N are 20,000, 100,000, and 200,000, respectively. For the GFB/NSA method, $L_x = 1$ and 3 are selected for comparison.

Figures 6 and 7 show the comparisons of the computational time/iteration and the total memory requirement of the GFB and

GFB/NSA methods. It is shown in Fig. 6 that the computational time/iteration of the GFB method is approximately $\mathcal{O}(N^2)$ while those of the GFB/NSA method for both L_x values are approximately $\mathcal{O}(N)$. In Fig. 7, the total memory requirement for all methods do not exhibit $\mathcal{O}(N)$ storage because in this example the dominant memory requirement comes from the fixed-size storage of the interaction within the unit-cell matrix $\bar{\bar{Z}}^{sg}$. Fig. 8 shows that without the storage of $\bar{\bar{Z}}^{sg}$, the memory requirement is $\mathcal{O}(N)$. Therefore, if planar periodic structures are larger in the x-direction and the storage of $\bar{\bar{Z}}^{sg}$ is relatively small compared to the overall storage, the memory requirement is expected to show $\mathcal{O}(N)$.

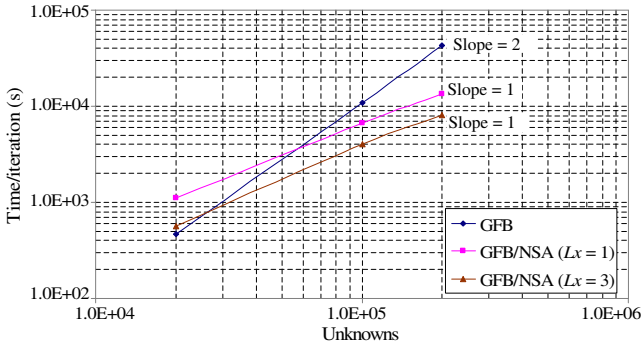

Figure 6. Computational time/iteration comparisons of the GFB and GFB/NSA methods with the separation index $L_x = 1$ and $L_x = 3$.

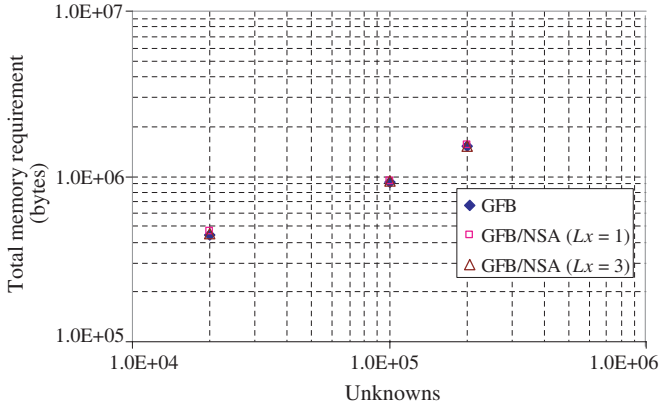

Figure 7. Total memory requirement comparisons of the GFB and GFB/NSA methods with the separation index $L_x = 1$ and $L_x = 3$.

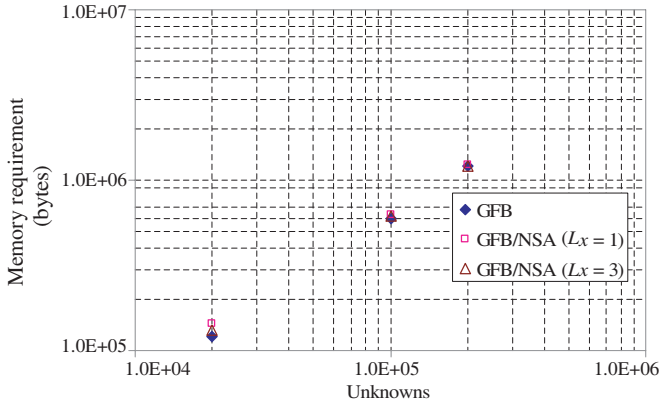

Figure 8. Comparisons of memory requirement without the unit-cell matrix storage of the GFB and GFB/NSA methods with the separation index $L_x = 1$ and $L_x = 3$.

Figure 9 shows the surface charge densities on the 500th patch for the 200,000 unknown case calculated by each method. This patch is on the top rightmost position in Fig. 1. It is shown from the figure that the surface charge densities are almost identical for all three calculations. They exhibit strong and weak densities at the edges and in the middle of the patch, respectively.

The surface charge densities for all patches calculated by the GFB/NSA methods are compared to those of the GFB method by the maximum error of each case. The maximum error, ε_ρ, of the surface charge densities is defined as

$$\varepsilon_\rho(\%) = \max_{n=1,2,\ldots,N} \left| \frac{\rho_n - \tilde{\rho}_n}{\rho_n} \right| \times 100, \tag{18}$$

where ρ_n and $\tilde{\rho}_n$ are the surface charge densities at the nth subelement calculated by the GFB and GFB/NSA methods, respectively. Table 2 shows that the surface charge densities calculated by the GFB/NSA method agree very well (within 1% accuaracy) with those from the GFB method for both L_x. The errors generated by using $L_x = 1$ and $L_x = 3$ are different because the integration limit and interval in k_ρ are different. As the number of unknown increases for a fixed L_x, both GFB/NSA calculations produce more discrepancies inferred from the increasing maximum errors. These results are to be expected since the same integral parameters in the spectral integration are used to cover more weak sources for these problems of interest.

Table 2. The maximum error (%) generated by the GFB/NSA methods compared to those from the GFB method.

Methods / Unknowns	GFB/NSA ($L_x = 1$)	GFB/NSA ($L_x = 3$)
20,000	0.06	0.07
100,000	0.20	0.19
200,000	0.28	0.31

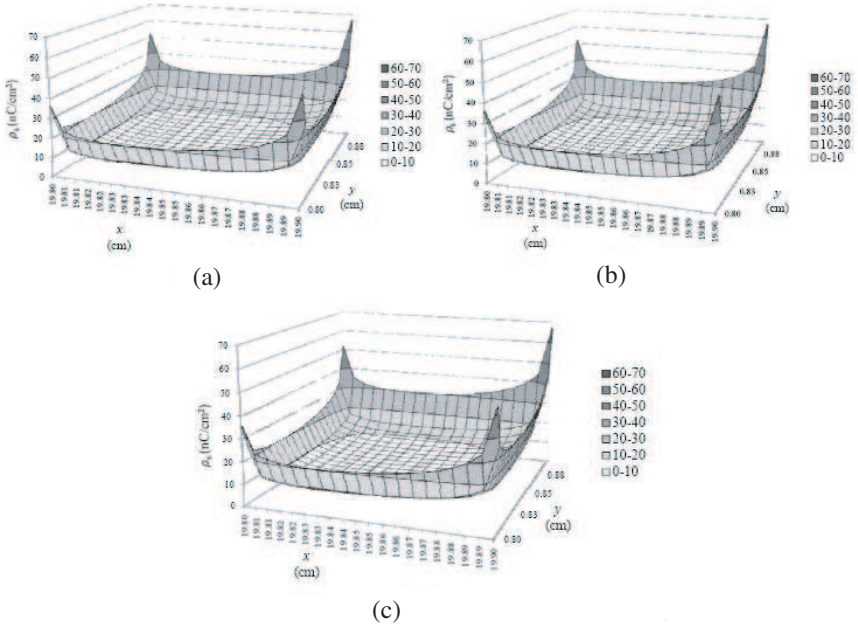

Figure 9. The surface charge densities on the 500th patch for the 200,000 unknown case calculated by (a) GFB, (b) GFB/NSA ($L_x = 1$), (c) GFB/NSA ($L_x = 3$).

6. CONCLUSION

The GFB/NSA method is applied to capacitance extraction problems of large finite planar periodic structures. The generalized forward-backward method allows the calculation of the interaction within a unit cell performed and stored beforehand. Thus, this procedure reduces the calculation performed in each iteration while increasing some memory storage. However, if planar periodic structures are very

large, the additional storage is negligible.

The interactions between unit cells are calculated by the GFB/NSA method to further accelerate the computational time. The contributions to a receiving element are separated into weak and strong source contributions by an appropriate separation index. The separation index is conveniently specified by an amount of unit cell rather than a distance. The strong source contribution is performed by the standard matrix-vector multiplication in the GFB method while the weak source contribution is computed using the NSA algorithm. Numerical results show good agreement between the commercial software [22], the GFB and GFB/NSA methods. Efficiency and accuracy of the GFB/NSA method is shown in the second example. With the array increment in one direction, the GFB and GFB/NSA methods show $\mathcal{O}(N^2)$ and $\mathcal{O}(N)$ in the calculation speed, respectively. The GFB/NSA method allows accuracy adjustment with the tradeoff in speed by appropriately controlling the number of integration points in the NSA algorithm. The memory requirement for very large problems tends to be $\mathcal{O}(N)$ if the associated matrix of a unit cell is small compared to the overall memory requirement. Thus, the GFB/NSA method is a promising method in analysis of large finite planar periodic structures. Future works will be focused on structures with dielectric layers.

REFERENCES

1. Itoh, T., R. Mittra, and R. D. Ward, "A method for computing edge capacitance of finite and semi-infinite microstrip lines," *IEEE Trans. Microwave Theory Tech.*, Vol. 20, 847–849, 1972.
2. Shu, W. and S. Xu, "Capacitance extraction for multiconductor transmission lines in multilayered dielectric media using the numerical Green's function," *Microwave and Optical Technology Letters*, Vol. 40, 529–531, 2004.
3. Nabors, K. and J. White, "FastCap: A multipole accelerated 3-D capacitance extraction program," *IEEE Trans. Computer-aided Design of Integrated Circuits and Systems*, Vol. 10, 1447–1459, 1991.
4. Nabors, K. and J. White, "Multipole-accelerated capacitance extraction algorithms for 3-D structures with multiple dielectrics," *IEEE Trans. Circuits Syst.*, Vol. 39, 946–954, 1992.
5. Jandhyala, V., E. Michielssen, and R. Mittra, "Multipole-accelerated capacitance computation for 3-D structures in a stratified dielectric medium using a closed-form Green's function,"

Int. J. Microwave Millimeter-wave Computer-aided Eng., Vol. 5, 68–78, 1995.

6. Phillips, J. R. and J. K. White, "A precorrected-FFT method for electrostatic analysis of complicated 3-D structures," *IEEE Trans. Computer-aided Design of Integrated Circuits and Systems*, Vol. 16, 1059–1072, 1997.
7. Zhu, Z., H. Ji, and W. Hong, "An efficient algorithm for the parameter extraction of 3-D interconnect structures in the VLSI circuits: Domain decomposition method," *IEEE Trans. Microwave Theory Tech.*, Vol. 45, 1179–1184, 1997.
8. Pan, Y. C., W. C. Chew, and L. X. Wan, "A fast mutipole-method-based calculation of the capacitance matrix for multiple conductors above stratified dielectric media," *IEEE Trans. Microwave Theory Tech.*, Vol. 49, 480–490, 2001.
9. Wang, C. F., L. W. Li, B. L. Ooi, P. S. Kooi, and M. S. Leong, "Fast capacitance computation based on adaptive integral solution of second-kind integral equation," *Journal of Electromagnetic Waves and Applications*, Vol. 16, No. 5, 711–728, 2002.
10. Yu, W. and Z. Wang, "Fast capacitance extraction of actual 3-D VLSI interconnects using quasi-multiple medium accelerated BEM," *IEEE Trans. Microwave Theory Tech.*, Vol. 51, 109–119, 2003.
11. Gope, D. and V. Jandhyala, "PILOT: A fast algorithm for enhanced 3D parasitic capacitance extraction efficiency," *Microwave and Optical Technology Letters*, Vol. 41, 169–173, 2004.
12. Sae-Heng, C. and D. Torrungrueng, "An application of the forward-backward (FB) method for capacitance extraction problems of planar structures," *Proceeding of IEEE TENCON 2004*, Vol. 4, 332–335, 2004.
13. Sae-Heng, C. and D. Torrungrueng, "Fast capacitance extraction for planar structures in free space using the novel spectral acceleration algorithm," *Proc. of the 2005 Asia-Pacific Microwave Conference*, Vol. 3, 1–4, 2005.
14. Lertsirimit, C. and D. Torrungrueng, "Fast capacitance extraction for planar structures in a layer medium using the novel spectral acceleration algorithm," *IEEE AP-S Intl. Symp. Digest*, San Diego, CA, July 2008.
15. Chou, H. T. and J. T. Johnson, "Formulation of forward-backward method using novel spectral acceleration for the modeling of scattering from impedance rough surfaces," *IEEE Trans. Geosc. Remote Sens.*, Vol. 38, 605–607, 2000.

16. Torrungrueng, D., H. T. Chou, and J. T. Johnson, "A novel acceleration algorithm for the computation of scattering from two-dimensional large-scale perfectly conducting random rough surfaces with the forward-backward method," *IEEE Trans. Geosc. Remote Sens.*, Vol. 38, 1656–1668, 2000.
17. Moss, C. D., T. M. Grzegorczyk, H. C. Han, and J. A. Kong, "Forward-backward method with spectral acceleration for scattering from layered rough surfaces," *IEEE Trans. Antennas and Propagation*, Vol. 54, 1006–1016, 2006.
18. Pino, M. R., L. Landesa, J. L. Rodríguez, F. Obelleiro, and R. J. Burkholder, "The generalized forward-backward method for analyzing the scattering from targets on ocean-like rough surfaces," *IEEE Trans. Antennas and Propagation*, Vol. 47, 961–969, 1999.
19. Pino, M. R., R. J. Burkholder, and F. Obelleiro, "Spectral acceleration of the generalized forward-backward method," *IEEE Trans. Antennas and Propagation*, Vol. 50, 785–797, 2002.
20. Lertsirimit, C. and D. Torrungrueng, "Fast capacitance extraction for finite planar periodic structures using the generalized forward-backward method," *IEEE AP-S Intl. Symp. Digest*, Charleston, SC, June 2009.
21. Harrington, R. F., *Field Computation by Moment Methods*, Wiley-IEEE Press, New Jersey, 1993.
22. Nikloic, M. M., A. R. Djordevic, and M. M. Nikloic, *ES3D: Electrostatic Field Solver for Multilayer Circuits*, Artech House, 2007.